

Spurs and feathering in spiral galaxies

C. L. Dobbs^{1*} and I. A. Bonnell¹

¹*School of Physics and Astronomy, University of St Andrews, North Haugh, St Andrews, Fife, KY16 9SS*

5th February 2006

ABSTRACT

We present Smoothed Particle Hydrodynamics (SPH) simulations of the response of gas discs to a spiral potential. These simulations show that the commonly observed spurs and feathering in spiral galaxies can be understood as being due to structures present in the spiral arms that are sheared by the divergent orbits in a spiral potential. Thus, dense molecular cloud-like structures generate the perpendicular spurs as they leave the spiral arms. Subsequent feathering occurs as spurs are further sheared into weaker parallel structures as they approach the next spiral passage. Self-gravity of the gas is not included in these simulations, stressing that these features are purely due to the hydrodynamics in spiral shocks. Instead, a necessary condition for this mechanism to work is that the gas need be relatively cold (1000 K or less) in order that the shock is sufficient to generate structure in the spiral arms, and such structure is not subsequently smoothed by the gas pressure.

Key words: galaxies: spiral – hydrodynamics – galaxies: structure – galaxies: ISM

1 INTRODUCTION

Understanding the gas dynamics in spiral galaxies is an important precondition if we are to comprehend the physics of star formation (Elmegreen (2002, 1999); Bonnell et al. (2006)) and galaxy evolution. The origin of spurs and feathering is one phenomenon that has proved difficult to explain. These features are commonly observed in many spiral galaxies, including grand design galaxies such as M51 (Aalto et al. (1999)). Spurs (particularly in M51) often show a correlation with HII regions, suggesting a link between these structures and star forming giant molecular clouds. In fact the local star-forming region of Orion has been referred to as the Orion spur (Bok1959). Therefore, understanding the origin of spurs may offer insights into the star formation process.

Spurs are seen as narrow dark lanes that extend perpendicular to the spiral arms (Lynds 1970; Weaver 1970). They are particularly striking in the HST images of M51 (Scoville et al. 2001), especially towards the centre of the galaxy. The spurs extend over half the distance between the arms, and are often dotted with HII regions. Surveys indicate that spurs have pitch angles of $30 - 50^\circ$ (Russell & Roberts 1992) and widths comparable to those of spiral arms (Elmegreen 1980). Further examples of spurs are also shown in Byrd (1983) (M31) and Kaufman et al. (1989) (M81).

We denote feathering (Balbus 1988; Kim & Ostriker 2002) by parallel filamentary features shifted from the spiral arms. These are often observed on the outskirts of spiral

galaxies (e.g. M74). Branches are more significant longer spurs often associated with resonances. Several simulations already have shown the bifurcation of spiral arms primarily at the 4:1 resonance of their potential (Patsis et al. 1994, 1997; Chakrabarti et al. 2003).

Spurs have been suggested to form mainly through gravitational or magneto-Jeans instabilities. Balbus (1988) demonstrated that transient gravitational stabilities develop preferentially nearly parallel and nearly perpendicular to the spiral arm. This introduces the appealing scenario where spurs and density perturbations along the arms are generated by the same mechanism. Generally, dense regions along the course of the spiral arm will produce projections roughly perpendicular to the arm as a result of shear expansion. Simulations by Kim & Ostriker (2002) show the formation and fragmentation of spurs in 2D magneto-hydrodynamical calculations of a shearing box. Dense clumps are produced in the arms principally through the magneto-Jeans instability, leading to the formation of spurs.

Previous numerical analysis by Dwarkadas & Balbus (1996) indicated that galactic flows through spiral arms are stable against purely hydrodynamic instabilities. However Wada & Koda (2004) have looked again at the non-self-gravitating, non-magnetic case, performing global simulations of a spiral galaxy. They observe a rippling distortion of the shock front and the formation of spurs at larger pitch angles. These spurs are interpreted as a consequence of Kelvin-Helmholtz instabilities.

We present hydrodynamic simulations which show the development of feathering and spurs in a spiral galaxy. These features are much more evident in our results than

* E-mail: cld2@st-and.ac.uk

previous purely hydrodynamical simulations. We note that most previous studies, including Wada & Koda (2004) and Dwarakadas & Balbus (1996), assume a high sound speed. Our analysis reveals that the temperature of the disk has a crucial effect on the disk structure and the formation of spurs. We show that these features are due to the shearing of structure in the spiral arms. Furthermore, inhomogeneities transmitted between the arms lead to the formation of new structure in the next arm.

2 CALCULATIONS

We use the 3D smoothed particle hydrodynamics (SPH) code based on the version by Benz (Benz 1990). The smoothing length is allowed to vary with space and time, with the constraint that the typical number of neighbours for each particle is kept near $N_{\text{neigh}} \sim 50$. Artificial viscosity is included with the standard parameters $\alpha = 1$ and $\beta = 2$ (Monaghan & Lattanzio 1985; Monaghan 1992).

2.1 Flow through galactic potential

The galactic potential includes a 4 armed spiral component, from Cox & Gómez (2002). The symmetric components consists of a logarithmic potential (e.g. Binney & Tremaine (1987)) that provides a flat rotation curve of $v_0 = 220 \text{ km s}^{-1}$, and a potential for the outer halo (Caldwell & Ostriker 1981). Parameters for the spiral part include the amplitude, 1 atom cm^{-3} , pattern speed, $2 \times 10^{-8} \text{ rad yr}^{-1}$ and pitch angle $\alpha = 15^\circ$ which are comparable with the Milky Way. The pattern speed leads to a co-rotation radius of 11kpc.

Overall the disk is in equilibrium, as the rotational velocities of disk particles balance the centrifugal force from the potential. This paper only considers how hydrodynamic forces and galactic potential influence the flow. In particular, self-gravity magnetic fields, heating, cooling or feedback from star formation are not included.

2.2 Initial conditions

Gas particles are initially chosen to occupy a region of radius $5 \text{ kpc} < r < 10 \text{ kpc}$. The disk also has a scale height $z \leq 100 \text{ pc}$. Particles are allocated positions and velocities determined from a 2D test particle run. The test particle run consists of 1 million particles initially distributed uniformly with circular velocities. They evolve for a couple of orbits subject to the galactic potential, to give a spiral density pattern with particles settled into their perturbed orbits. For the highest resolution run (4 million particles), 4.5×10^5 test particles were split into 9 particles each.

In the SPH initial conditions, the particles are given velocities in the z direction from a random Gaussian distribution of 2.5% of the orbital speed. The same magnitude velocity dispersion is also added to the x and y velocities. The gas is distributed uniformly on large scales with an average surface density of $\Sigma \approx 2 \text{ M}_\odot \text{ pc}^{-2}$, although it is somewhat clumpy on smaller scales. The densities in the interarm regions range from $10^{-25} \text{ g cm}^{-3}$ to $10^{-24} \text{ g cm}^{-3}$. The total mass of the disk is $5 \times 10^8 \text{ M}_\odot$.

The number of particles is either 10^6 or 4×10^6 . The

higher resolution work was carried out on UKAFF (UK Astrophysical Fluids Facility). Simulations were run for between 200 and 300 Myr, where the orbital period at 5 kpc is 150 Myr. No boundary conditions are applied to our calculations.

All calculations are isothermal with temperatures of 50, 10^2 , 10^3 , or 10^4 K. Most previous simulations and analysis of spiral galaxies (e.g. Wada & Koda (2004); Gittins (2004); Kim & Ostriker (2002); Dwarakadas & Balbus (1996)) assume a sound speed of approximately 10 km s^{-1} corresponding to the hotter (10^4 K) component of the ISM. However, for GMCs to form, gas entering the spiral arms must be cold atomic clouds (Elmegreen 2002) or pre-existing molecular gas (Pringle et al. 2001). Since our initial aim of this work was to investigate molecular cloud formation (described in Dobbs et. al. 2006), lower ISM temperatures were adopted for these calculations.

3 RESULTS

The highest resolution run used 4×10^6 particles, giving a resolution of 125 M_\odot per particle. The temperature in this simulation was 50 K. Density plots at 4 different times are shown in Fig. 1. These and subsequent figures are shown in the rotating frame of the spiral potential.

Initially there is a smooth spiral perturbation to an approximately uniform disk. For the 50 K gas, the spiral arms are initially very thin. The density of the spiral arms increases with time and non-uniform structure develops along each arm. As this arm substructure grows, dense clumps shearing away from the spiral arms lead to interarm features. These features occur on the leading side of the spiral arm, leaving the trailing side smooth. Structure on the outside of spiral arms is noticeable first in the inner parts of the disk (Fig. 1b), and then spreads to larger radii. This is not surprising since the orbital period is less for smaller radii, so the comparative evolution of that part of the disk is faster. Both the arm and interarm regions become more disordered with time, and consequently the spiral arms become wider.

Further runs have been performed at 100, 10^3 and 10^4 K with 1 million particles and are shown in Fig. 2. As the temperature increases, the Mach number of the shock decreases and much weaker spiral arms are produced. The gas is largely smooth at 10^4 K due to the higher pressure, and the spiral arms exhibit no obvious substructure.

The detailed structure of the spurs and feathering in the 50 K simulation is shown in Fig. 3. We see that the interarm structure increases with time from smaller scale structures to more pronounced larger scale spurs and feathering. Over time, spurs become more distinct with a regular spacing ($\approx 0.7 \text{ kpc}$ after 160 Myr in Fig. 3c). Furthermore, we see that there is a direct correlation between the spurs that leave perpendicular to the spiral arm and the feathering that approaches the next spiral arm. The feathering here has the appearance of closely spaced parallel lanes of gas with a much smaller pitch angle than apparent for spurs. The interarm structure in the 1000 K run is also shown in Fig. 2b. The spurs, and to a lesser extent the feathering, are still evident but are less pronounced. As noted above, the 10^4 K simulation does not display such interarm structure, but instead retains a smooth gas distribution (Fig. 2c).

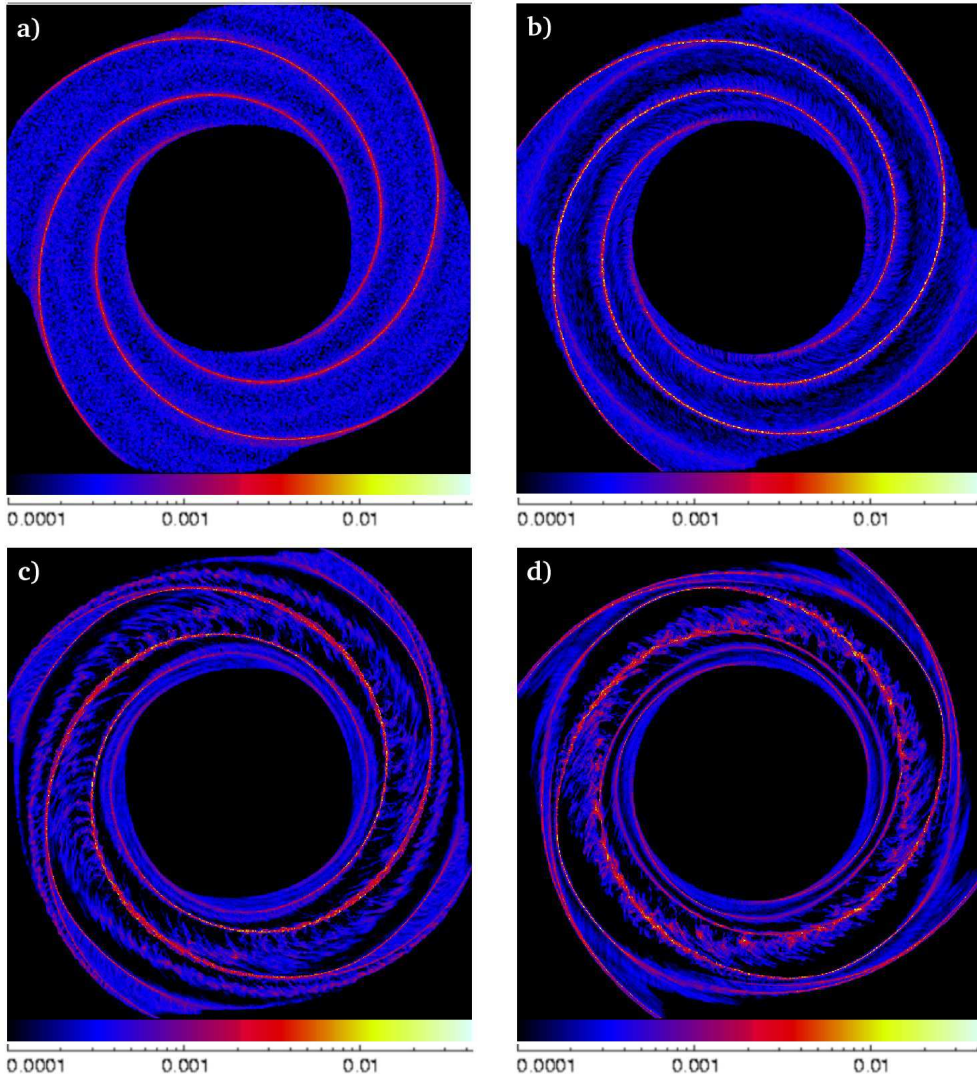


Figure 1. Column density plots (g cm^{-2}) when $T=50$ K after a) 0, b) 60, c) 160 and d) 260 Myr. The number of particles is 4 million and each plot is 20 kpc by 20 kpc. The same scaling is used on all subsequent column density plots.

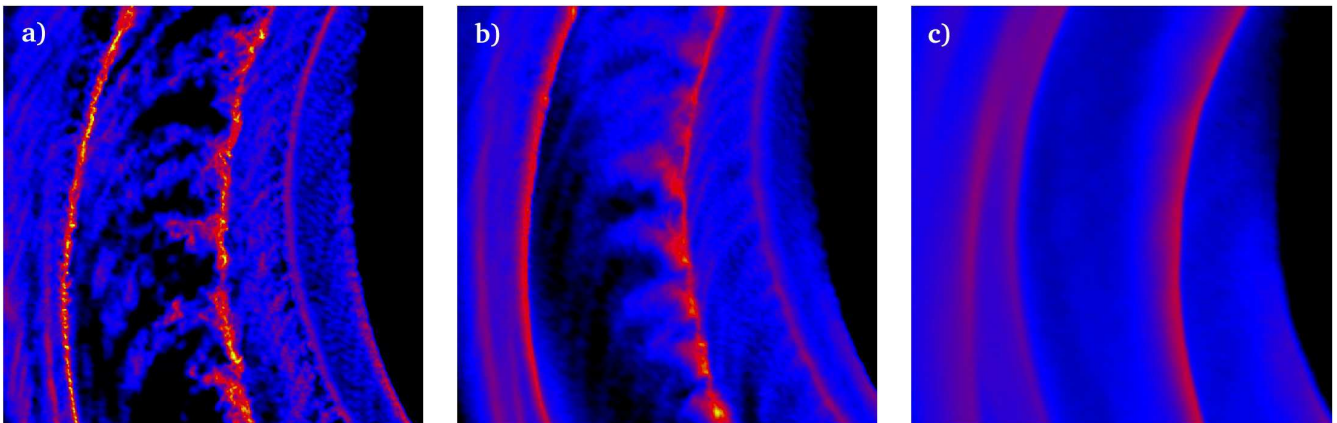


Figure 2. Column density plots (g cm^{-2}) when the temperature is a) 100, b) 10^3 and c) 10^4 K. The time corresponding for each figure is 220 Myr. Each plot shows a 5 kpc by 5 kpc section of the global simulation. The overall number of particles in these simulations is 1 million.

3.1 Formation of spurs

In order to ascertain the origin of the interarm structure, we have traced the gas backwards in time from the spur that leaves the spiral arm to when the gas was located in the spiral arm itself. Figs. 4 and 5 show that there is a direct correlation between clumps in the spiral arms and the spurs that leave perpendicular to the arms. Thus we can conclude that the spurs are simply the shearing of clumps in the spiral arms, due to the divergent orbits of material that leave the arm. As structure (GMCs) is observed to exist in spiral arms, this provides a simple explanation for the presence of spurs. Further shearing then produces the feathering from the spurs. A similar scenario is discussed in Gittins (2004), who also describes the formation of spurs in SPH calculations.

The clumpy structure of the spiral arms is due to the dynamics as the ISM passes through a spiral shock (Dobbs et al. 2006). We interpret the growth of clumpy structure in the spiral arms in terms of the particles' change in angular momenta in the shock, which modifies the velocity phase space distribution of particles in the disk. The particles enter the shock at non-uniform intervals of space or time (since the interarm regions are not homogeneous). As they subsequently gain and/or lose angular momentum in the spiral arms, the particles tend to group together in velocity space (Dobbs et al. 2006). Hence the inhomogeneities of the initial gas distribution are amplified in the spiral arms and clumps form. We estimate the spacing of these clumps from the time particles spend in the spiral arm ($t_{arm} \sim 6 \times 10^7$ years) and the typical velocity spread ($v_{\perp} \sim 10 \text{ km s}^{-1}$) (Dobbs et al. 2006) to be $L \sim t_{arm} v_{\perp} \sim 600 \text{ pc}$.

We plot the paths of five particles and their corresponding angular momenta in Fig. 6. Since the spiral arms are regions of significantly enhanced density, gas particles from a range of radii must interact in the shock. Particles entering the shock on epicyclic paths are typically at the furthest extent of their orbit. They therefore encounter higher angular momentum material already in the shock (e.g. red line, Fig. 6). This generally leads to a jump in the angular momentum of the particles as they enter the shock (e.g. yellow line, Fig. 6). As particles travel along the spiral arm, they tend to lose angular momentum, since they are constrained by the spiral potential. It appears in Fig. 6 that particles entering the shock later (e.g. green line) show less change in angular momentum, possibly because they interact with gas in the shock which has similar angular momentum. Hence the path represented by the green line is less affected by the shock, and this particle spends less time in phase with the potential compared to the others. Eventually the gas leaves the spiral arm when its angular momentum is too high to travel further radially inwards, and forms the spur shown in Figure 4.

This model also explains why less structure is apparent in the higher temperature simulations. At higher ISM temperatures, the shocks are weaker and they have less effect on the particles' angular momentum. The particles spend a shorter time in phase with the potential and their orbits are less perturbed. Overall the distribution of the angular momenta of particles remains much more uniform (Dobbs et al. 2006). Furthermore, the gas pressure can smooth out much of the structure during the crossing of the spiral arm. If the

structure in the spiral arms is removed, then there is nothing to shear into the subsequent spurs and feathering in the interarm region. For example, the 10^4 K run has a sound speed of $\approx 10 \text{ km s}^{-1}$ which is comparable to the velocity of the gas perpendicular to the spiral arm (in the rotating spiral potential). Thus, structures of size scales \leq the width of the arm can be smoothed by the internal pressure before leaving the spiral arm.

An alternative explanation is that the spiral arm structure arises from Kelvin Helmholtz instabilities (Wada & Koda 2004). We find that the Reynolds numbers for our simulations are relatively low ($Re \approx 500$ for 100 K gas due to the numerical resolution) implying that the resolution is insufficient for Kelvin Helmholtz instabilities to occur. Interestingly, Wada & Koda (2004) find spurs forming from hot (10^4) gas, although their analysis likewise shows that increasing the Mach number of the shock (corresponding to a lower temperature) increases the susceptibility of gas disks to hydrodynamic instabilities.

4 CONCLUSION

We have performed numerical simulations of disks in spiral galaxies which demonstrate the widespread formation of spurs and feathering. The overall appearance of the galactic disk, enhanced by these features, is remarkably similar to observations of galaxies such as M51 and M81. In addition, the properties of individual spurs (pitch angle, dimensions) are comparable with observations.

The formation of spurs and feathering in the interarm regions of spiral galaxies is shown to be linked to the presence of structure in the spiral arms. These findings concur with similar work by Gittins (2004). Upon leaving the spiral arms, dense concentrations of gas are sheared by diverging orbits. Spurs form perpendicular to the spiral arms, which later become feathering that impacts into the next spiral arm. The formation of spurs and GMCs are thus directly related, since these denser structures in the spiral arms are the sites of molecular clouds.

The necessary conditions for interarm features to form are density inhomogeneities and relatively cold gas ($T \lesssim 1000 \text{ K}$). A clumpy ISM allows structure growth in cold spiral shocks. Such structure formation in the spiral arms, and therefore spur formation, does not occur in our simulations when the gas is hot.

ACKNOWLEDGEMENTS

Computations included in this paper were performed using the UK Astrophysical Fluids Facility (UKAFF).

REFERENCES

- Aalto S., Hüttmeister S., Scoville N. Z., Thaddeus P., 1999, *ApJ*, 522, 165
- Balbus S. A., 1988, *ApJ*, 324, 60
- Benz W., 1990, in *Numerical Modelling of Nonlinear Stellar Pulsations Problems and Prospects Smooth Particle Hydrodynamics - a Review*. pp 269–+

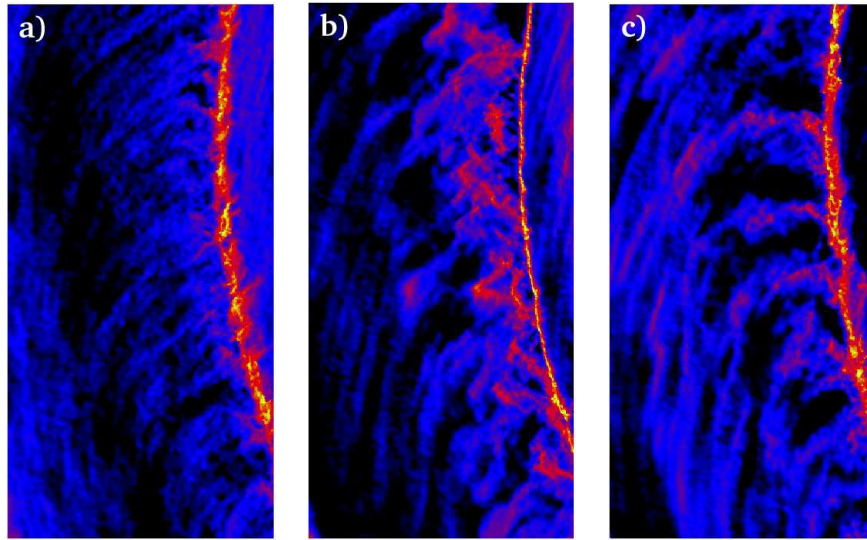


Figure 3. Time evolution of feathering and spurs. Column density plots for the 50 K run after a) 80 Myr, b) 120 Myr and c) 160 Myr. Each plot is 2 kpc by 4 kpc.

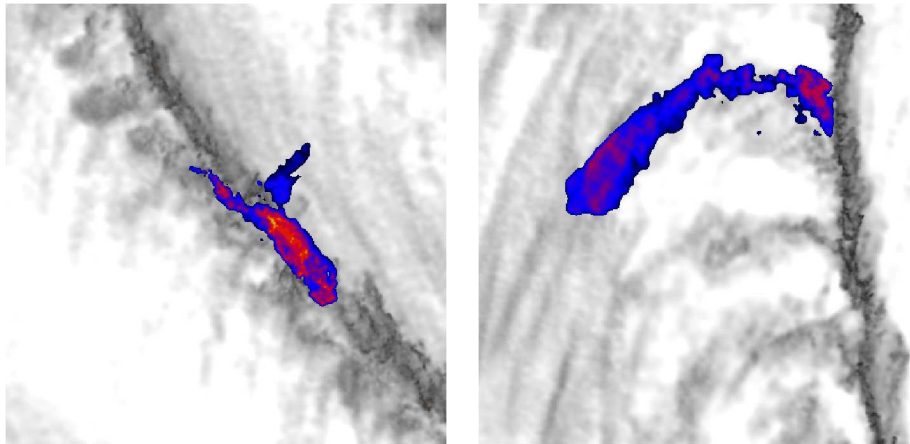


Figure 4. Formation of a spur (right hand plot, after 160 Myr) from a dense clump of gas in the spiral arm (left hand plot, after 100 Myr). The temperature is 50 K and both plots are 2 kpc by 2 kpc.

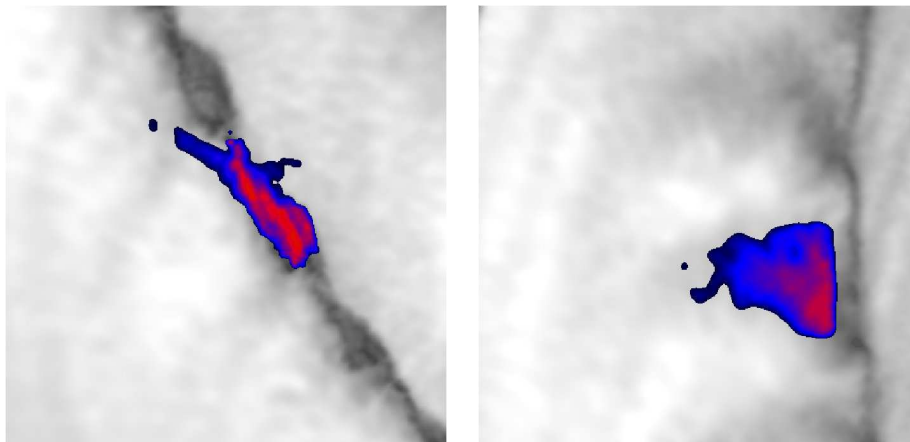


Figure 5. Formation of a spur (right hand plot, after 220 Myr) from a dense clump of gas in the spiral arm (left hand plot, after 180 Myr). The temperature is 1000 K and both plots are 2 kpc by 2 kpc.

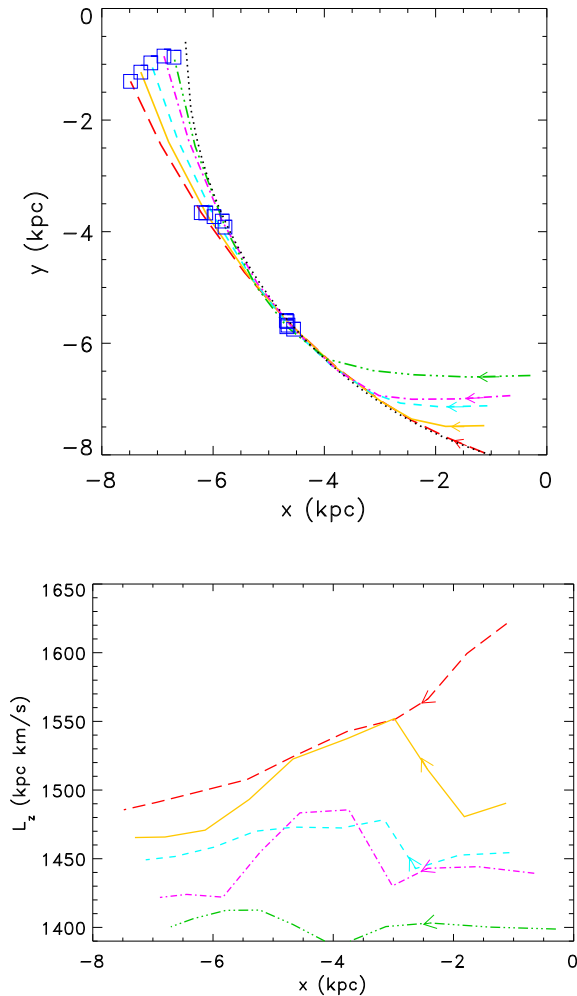


Figure 6. The orbits of 5 selected particles are displayed pre- and post-shock (top) where the xy-coordinates correspond to a fixed Cartesian grid centred at the midpoint of the disk. The dotted line indicates the position of the shock front, and the orbits are taken from the rest frame of the potential. Boxes indicate the location of the five particles at three corresponding times. The final position of the particles coincide with the spur shown in Figure 4 (right). The corresponding angular momenta of the particles are also plotted (bottom). Particles are travelling from right to left in both plots.

Binney J., Tremaine S., 1987, *Galactic dynamics*. Princeton, NJ, Princeton University Press, 1987, 747 p.
 Bonnell I. A., Dobbs C. L., Robitaille T. P., Pringle J. E., 2006, *MNRAS*, 365, 37
 Byrd G. G., 1983, *ApJ*, 264, 464
 Caldwell J. A. R., Ostriker J. P., 1981, *ApJ*, 251, 61
 Chakrabarti S., Laughlin G., Shu F. H., 2003, *ApJ*, 596, 220
 Cox D. P., Gómez G. C., 2002, *ApJS*, 142, 261
 Dobbs C. L., Bonnell I. A., Pringle J. E., 2006, in *MNRAS* submitted
 Dwarkadas V. V., Balbus S. A., 1996, *ApJ*, 467, 87
 Elmegreen B. G., 1999, in *Star Formation 1999, Proceedings of Star Formation 1999, held in Nagoya, Japan, June 21 - 25, 1999*, Editor: T. Nakamoto, Nobeyama Radio Ob-

servatory, p. 3-5 *Star Formation in Galaxies*. pp 3-5
 Elmegreen B. G., 2002, *ApJ*, 577, 206
 Elmegreen D. M., 1980, *ApJ*, 242, 528
 Gittins D. M., 2004, Ph.D. Thesis, Cambridge University
 Kaufman M., Bash F. N., Hine B., Rots A. H., Elmegreen D. M., Hodge P. W., 1989, *ApJ*, 345, 674
 Kim W., Ostriker E. C., 2002, *ApJ*, 570, 132
 Lynds B. T., 1970, in *IAU Symp. 38: The Spiral Structure of our Galaxy The Distribution of Dark Nebulae in Late-Type Spirals*. pp 26-+
 Monaghan J. J., 1992, *ARA&A*, 30, 543
 Monaghan J. J., Lattanzio J. C., 1985, *A&A*, 149, 135
 Patsis P. A., Grosbol P., Hiortelis N., 1997, *A&A*, 323, 762
 Patsis P. A., Hiortelis N., Contopoulos G., Grosbol P., 1994, *A&A*, 286, 46
 Pringle J. E., Allen R. J., Lubow S. H., 2001, *MNRAS*, 327, 663
 Russell W. S., Roberts W. W., 1992, *ApJ*, 398, 94
 Scoville N. Z., Polletta M., Ewald S., Stolovy S. R., Thompson R., Rieke M., 2001, *AJ*, 122, 3017
 Wada K., Koda J., 2004, *MNRAS*, 349, 270
 Weaver H. F., 1970, in *IAU Symp. 39: Interstellar Gas Dynamics Some Characteristics of Interstellar Gas in the Galaxy*. pp 22-+

This paper has been typeset from a \TeX / \LaTeX file prepared by the author.